Structural Eng./Earthquake Eng., JSCE, Vol.24, No.2, 123s-130s, 2007
(Translated from a paper which originally appeared on Journal of Applied Mechanics, JSCE, Vol.8, pp.601-608, 2005.8)

DEVELOPMENT OF LAT-PIV VISUALIZATION TECHNIQUE FOR PARTICLE-FLUID SYSTEM

Hidetaka SAOMOTO[1], Takashi MATSUSHIMA[2] and Yasuo YAMADA[3]

[1]Member of JSCE, National Institute of Advanced Industrial Science and Technology
(1-1-1, Higashi, Tsukuba, Ibaraki 305-8567, Japan)
E-mail:h-saomoto@aist.go.jp
[2]Member of JSCE, Associate Professor, Dept. of Engineering Mechanics and Energy, University of Tsukuba
(1-1-1, Tennodai, Tsukuba, Ibaraki 305-8573, Japan)
E-mail:tmatsu@kz.tsukuba.ac.jp
[3]Member of JSCE, Professor, Dept. of Engineering Mechanics and Energy, University of Tsukuba
(1-1-1, Tennodai, Tsukuba, Ibaraki 305-8573, Japan)
E-mail:yamada@kz.tsukuba.ac.jp

Mechanical behavior of particle-fluid systems is extensively studied in various engineering field such as geotechnical engineering, mechanical engineering and powder technology. Although observation of complicated behaviors including interaction between particles and pore fluid is essential, very few efficient techniques are available for this purpose. From this point of view an observation technique based on LAT (Laser-Aided Tomography) and PIV (Particle Image Velocimetry) was developed and applied to the permeability experiments involving a seepage failure. The LAT-PIV technique enables us to visualize not only the particle motion but also the pore fluid motion and evaluate them quantitatively.

Key Words : *visualization, LAT-PIV, particle-fluid system*

1. INTRODUCTION

The mechanical behavior of particle-fluid system plays important role in various engineering problems. In the field of geotechnical engineering, such phenomena as boiling, piping and liquefaction are of this type that are induced by the interaction between soil particles and pore fluid. It is essential but substantially difficult for us to observe the internal behavior of such phenomena. Few visualization techniques available are classified into two types depending on whether they use visible ray or invisible ray.

The latter is more common and the X-ray CT is one of popular methods of this type. This method is very useful to visualize the void distribution and the progress of shear band in geo-materials[1), 2)]. Kobayashi et al.[3)] visualized sand particle-pore water system by the X-ray CT; however, it was impossible to visualize the flow of pore water because of the homogeneity of its density.

Another well known method using invisible ray is the MRI; however, it is costly and ineffective in time resolution.Ogawa et al.[4)] employed the high-resolution MRI to measure the three-dimensional fluid velocity in a porous medium composed of glass grains.

In the field of fluid mechanics, visible ray such as laser light is widely used for PIV (Particle Image Velocimetry), where some optically-designed specimen is usually employed for internal visualization. To investigate the kinetic properties of fluid flow in a thermal converter, Matsui et al.[5)] measured pore fluid velocity passing through void structure formed by many pyrex glass spheres. Sakakibara et al.[6)] revealed the flow pattern caused by a swimming fish behavior using the stereo-PIV, which is noteworthy for capturing both solid (fish) and fluid behaviors. As mentioned above, most studies using PIV have not focused on the solid movement but on the fluid behavior.

In this study, we developed a new technique LAT-PIV, combining LAT (Laser-Aided Tomography)[7), 8), 9)] and PIV for visualizing both movement of solid particles and fluid flow, then examined the applicability of the LAT-PIV by a series of permeability tests including seepage failure. The LAY-PIV technique proved to be successful in measuring the

mean fluid velocity-hydraulic gradient relationship and the fluid velocity passing through the pore structure, as well as in visualizing the movement of particles and the behavior of fluid during seepage failure.

2. LAT-PIV TECHNIQUE

The LAT-PIV technique, combining LAT and PIV, was developed for visualizing both movement of particles and fluid flow.

LAT, a kind of laser-slicing method and originally developed by Konagai et al.,[7] visualizes each particle motion including rotation inside a 3-D specimen composed of crushed glass whose pore is filled with fluid of the same refractive index as the grains. LAT has been effectively applied to such practices in visualizing micro-structure of granular material[8] and analyzing progressive development of shear band in granular medium[9]. In the present study, two kinds of silicone oil with different refractive indexes, HIVAC-F-4 and KF-56 (Shin-Etsu Chemical Co., Ltd.), were interblended in the volume ratio of about 2 to 5, which attained the same refractive index with particles. By passing laser sheet through the LAT specimen, the surface edges of glass grains are captured as contours gleaming green in the laser sheet.

PIV, also a kind of laser-slicing method, visualizes fluid motion by pursuing a pattern created by tracing powder mixed into the fluid. The diameter of tracing powder is almost a few dozen microns. The fluid velocity field is quantitatively obtained by carrying out a pattern matching image processing with respect to the flecks of tracing powder.

Figure 1 shows a schematic illustration of the observation system used in this study and the overview of a LAT-PIV specimen. The specimen possesses features required by both LAT and PIV. A newly developed measuring system, consisting of a CCD monochrome camera (1 million pixels, 500 FPS (frames/sec), Motionpro, REDLAKE) and a PC, is able to take photographs in digitized form for almost 10 seconds with 500 FPS as the marginal performance.

Figure 2 shows a photograph taken by the LAT-PIV technique with numerous tracing powders (flecks) and cross sections of the glass grains (no pattern regions) on the laser sheet produced by expanding the green laser beam (58-GSS-305, MELLES GRIOT).

To separate the pore fluid area from the LAT-PIV image and improve the accuracy of image processing, fluorescent powder that gleams pale orange on the green laser sheet and green-cut filter were employed here. The fluorescent powder[10] is easily produced by staining ordinary powder used in PIV with aqueous solution of rhodamine 6G.

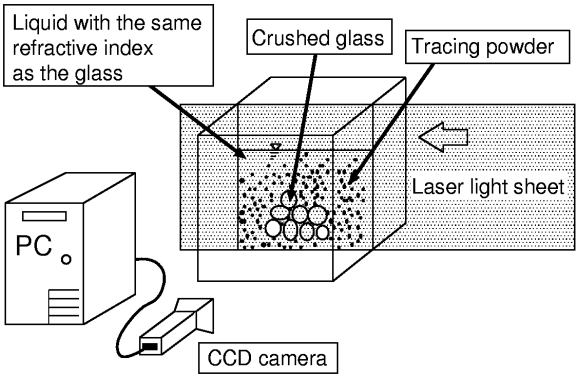

Fig.1 Brief overview of observation system.

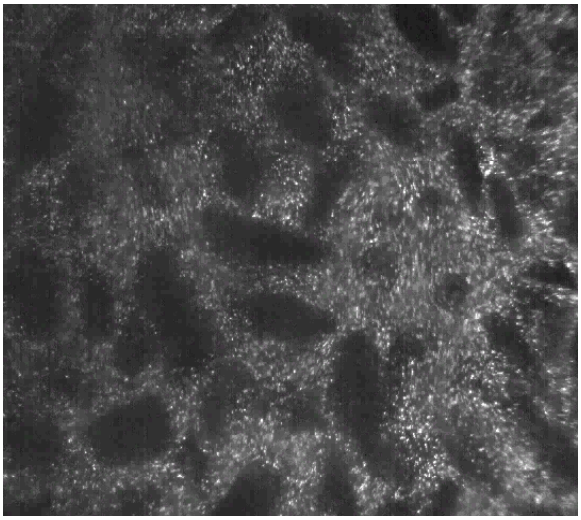

Fig.2 Snap shot by LAT-PIV.

3. VISUALIZATION OF PERMEABILITY TEST AND SEEPAGE FAILURE WITH LAT-PIV

(1) Experimental apparatus and material properties

In order to investigate the applicability of the LAT-PIV, a series of permeability tests including seepage failure was conducted. **Figure 3** indicates a schematic diagram of the experimental apparatus and **Table 1** lists the material properties.

The apparatus had a circulation loop for the silicone oil which flows upward from the bottom of the loosely packed specimen made by a pluviation method. Wire mesh filters (1mm grid) placed close to the inlet zone were designed to avoid a local seepage failure caused by non- rectified inflow. Two pressure

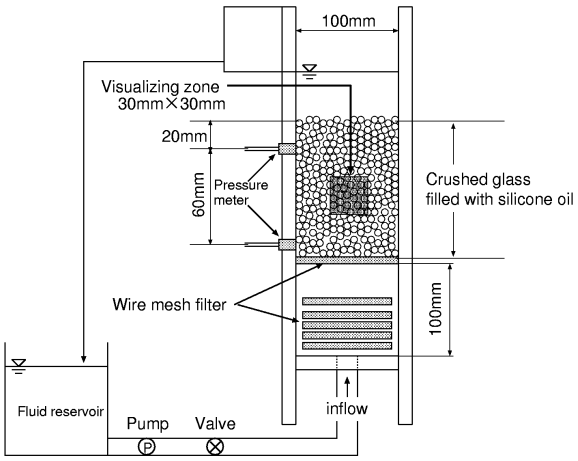

Fig.3 Schematic diagram of experimental apparatus.

Table 1 Material properties.

	Silicone oil	Glass grain	Tracing powder
Density (g/m^3)	1.02	2.52	1.02
Diameter		2 -5 mm	40 μm
Viscosity	20.6 mm^2/s		
Refractive Index	1.514	1.514	

meters were set on the side wall to obtain the hydraulic gradient.

(2) Experimental procedures and shutter speeds

The experimental procedures were as follows:

1) Pump the silicone oil into the specimen by opening the valve, and then keep the valve open to stabilize the outflow with a constant rate.
2) After the stabilization, measure the pressure gradient and the mass of outflow.
3) Visualize the interior of the specimen with the LAT-PIV during the steady state.
4) Increase the flow rate slightly, and repeat the procedures 1) to 3) step by step.

The experiment comprised 20 stages from the seepage state to the boiling state with increasing flow rate. During the experiment, the laser light sheet always passed through 3cm inside the specimen with the same intensity and hundreds of cross-sectional digital images were taken at each stage where the FPS and shutter speeds listed in Table 2 were configured.

Table 2 FPS and shuter speeds at each stage.

	Hydraulic gradient	FPS	Shutter speed (s)
No.1	0.030	60	1/480
No.2	0.078	100	1/700
No.3	0.113	125	1/875
No.4	0.161	200	1/800
No.5	0.217	250	1/750
No.6	0.258	250	1/750
No.7	0.308	250	1/750
No.8	0.347	250	1/750
No.9	0.395	400	1/800
No.10	0.437	400	1/800
No.11	0.485	400	1/800
No.12	0.545	400	1/800
No.13	0.608	500	1/500
No.14	0.712	500	1/500
No.15	0.606	500	1/500
No.16	0.670	500	1/500
No.17	0.650	500	1/500
No.18	0.637	500	1/500
No.19	0.653	500	1/500
No.20	0. 685	500	1/500

4. RESULTS OF EXPERIMENT

(1) Mean fluid velocity vs. hydraulic gradient

Figure 4 plots the relationship between the mean fluid velocity and the hydraulic gradient obtained by the experiment. The data points are clearly divided into two regions: one corresponds to the seepage state (stage No. 0 - No.14) and the other to the boiling state (stage No.15 - No. 20).

As can be seen in this figure, the mean fluid velocity abruptly increased around the hydraulic gradient value of 0.7, which indicates the occurrence of boiling within the specimen. Accordingly, the value 0.71 measured at stage No. 14 in Table 2 can be regarded as the critical hydraulic gradient. This value was comparable but a little smaller compared with the theoretical range from 0.78 to 0.92 corresponding to the maximum and the minimum void ratios, i.e. 0.90 and 0.59, respectively. In contrast to this result,

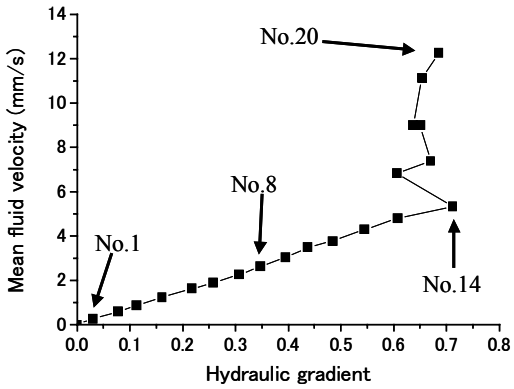

Fig.4 Plot of vertical mean fluid velocity v.s. hydraulic gradient.

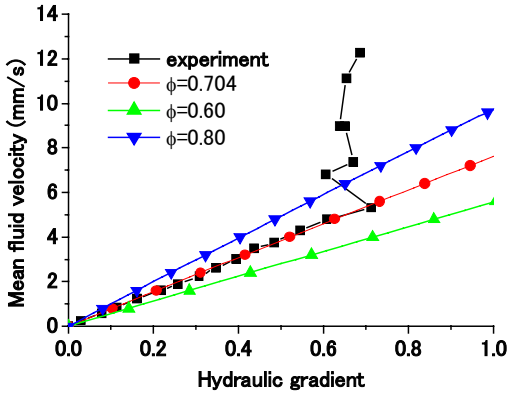

Fig.5 Vertical mean fluid velocity v.s. hydraulic gradient with the fitting results of the Ergun's equation.

the critical hydraulic gradient measured for another specimen made with bigger glass grains from 5 to 10 mm in diameter was definitely smaller than the theoretical range because of its high perviousness.

Within the stage from No. 0 to No. 14, a linear relationship existed between the mean fluid velocity and the hydraulic gradient, which represents the Darcy's law. The coefficient of permeability obtained from the slope of the line was 7.68×10^{-1} cm/s. In the field of geotechnical engineering, Hazen's equation or Taylor's equation are well known and often used for the estimation of permeability; however, these equations may not fit well such cases as this experiment, where the particle shape and fluid viscosity are considerably different from ordinary geomaterials. The measured permeability, therefore, was compared with that calculated by an enhanced version of Darcy's law, known as Ergun's equation[11]. The Ergun's equation, obtained on the assumption that the viscous losses and the kinetic energy losses are additive, covers the entire range of flow rates, and is widely referred in chemical engineering. Since the Ergun's equation takes account of viscosity, density and porosity as well, it can be easily applicable to a special pore fluid like silicone oil. The Ergun's equation is given as follows:

$$i=\frac{150\mu(1-\varepsilon)^2}{\rho g(\phi d_m)^2\varepsilon^3}v+\frac{1.75(1-\varepsilon)}{g(\phi d_m)\varepsilon^3}v^2 \qquad (1)$$

where the notations i and v indicate the hydraulic gradient and the mean fluid velocity; μ and ρ correspond to the viscosity and the density of the fluid; ε is the porosity and ϕ and d_m are sphericity and diameter of the grains, respectively; g is the acceleration of gravity.

By substituting the values listed in **Table 1** and the maximum porosity into this equation, then the sphericity only remains uncertain for evaluating the hydraulic losses. According to the list of the sphericity[12), 13)], most kinds of grains often encountered in engineering fields are within the range from 0.6 to 0.8: e.g. 0.65 for crushed glass, 0.83 for rounded sand. **Figure 5** shows the relationship between the mean fluid velocity and the hydraulic gradient obtained from the Ergun's equation for different values of sphericity.

As can be seen in **Fig.5**, the Ergun's equation assuming the sphericity value of 0.704, yielded a good agreement with the experimental result within the seepage stages. This value was, however, a little greater than the reference value of 0.65 for glass grains subjected to abrasion by means of ball milling. The Ergun's equation gave the possible values of permeability bounded by the upper and the lower lines with triangle marks, which corresponded to the range from 5.53×10^{-1} cm/s to 9.76×10^{-1} cm/s. However, it is to be noted that the Ergun's equation can not predict the drastic change in the permeability due to boiling.

(2) Pore fluid flow patterns obtained by image analysis

Figures 6, 7 and **8** represent the distributions of fluid velocity vectors inside the specimen at stage No.1, No.8 and No.14 indicated in **Fig.4**, respectively. To obtain these figures, a PIV image analysis with a sub-pixel accuracy was employed.

In the image analysis, the magnifying power was set at 5.53×10^{-2} mm/pixel, and then 33 pixel (1.82mm) square template was used as a pattern matching area. The fluid velocity vectors were measured at 7885 points for each image with a lattice-like arrangement; the values of color indexes indicated the norms of the velocity vectors in terms of millimeter per second.

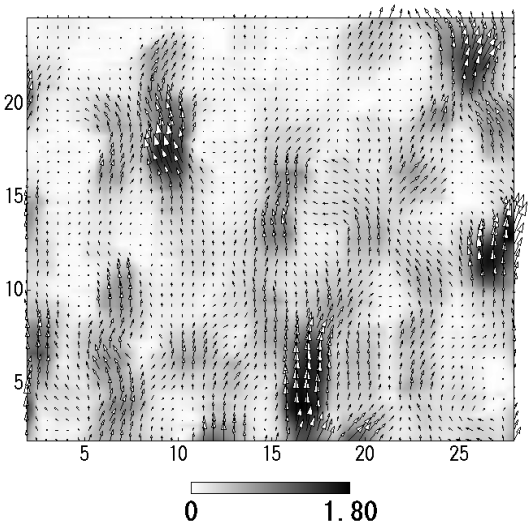

Fig.6 Distribution of fluid velocity at stage No.1, 60FPS.

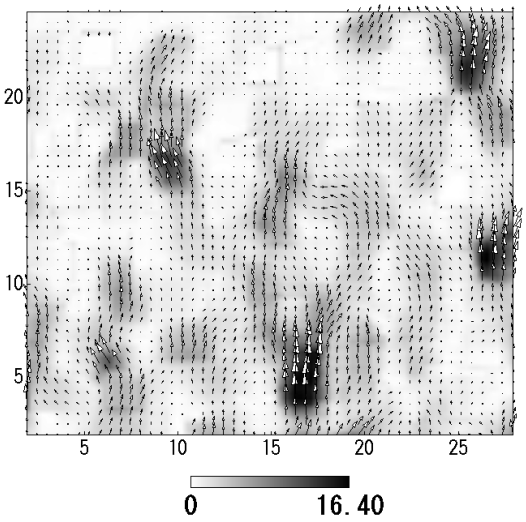

Fig.7 Distribution of fluid velocity at stage No.8, 250FPS.

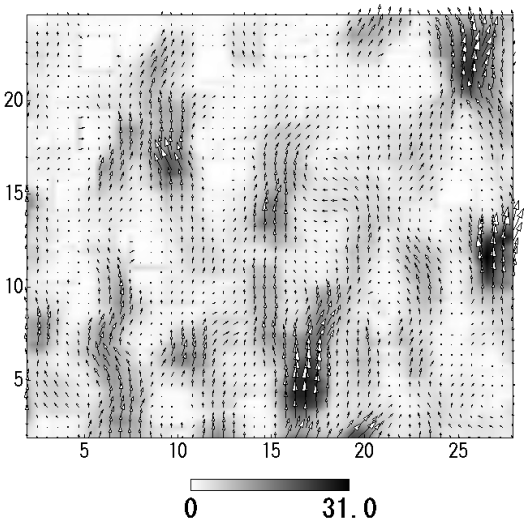

Fig.8 Distribution of fluid velocity at stage No.14, 500FPS.

Although these figures were found lacking in uniformity, the region of faster flow always appeared at almost similar spot at each stage within seepage state, which may suggest an immutability of the pore structure.

Figure 9 compares the relationship between the vertical mean fluid velocity and the hydraulic gradient between the values obtained from actual measurement and the image analysis. The disjunction appeared to initiate at the hydraulic gradient value of around 0.2, then the velocity obtained from image analysis decreased to 80 % of that actually measured at stage No.14 ($i = 0.712$). This disjunction may be attributed to the effects of shoot interval and the fact that the measurement was made only on a single cross section.

As indicated in **Fig.6**, **7** and **8**, the velocity vectors had wide range of norms; therefore the multi time scale PIV image analysis might be more suitable than the ordinary PIV image analysis using a unitary time interval. Although the shooting interval of camera in an experimental stage was fixed at a constant value (Δt), we could perform a set of ordinary PIV image analyses, each with a different time interval from others, based on the same data. For stage 14, ordinary PIV analyses were conducted using 10 different values of time interval ranging from Δt to $18\,\Delta t$, then all results were merged into a vector diagram. As a consequence of the multi time image analysis, the vertical mean velocity of 4.36 mm/s was acquired. Although the mean velocity increased a little from 4.25 mm/s obtained by the ordinary PIV image analysis, it was considerably small compared with the measured value of 5.31 mm/s. This implies the average velocity on other planes than the measured one may have been much higher.

Figure 10 shows the histograms of the vertical velocity components for stage No. 1, No. 8 and No.

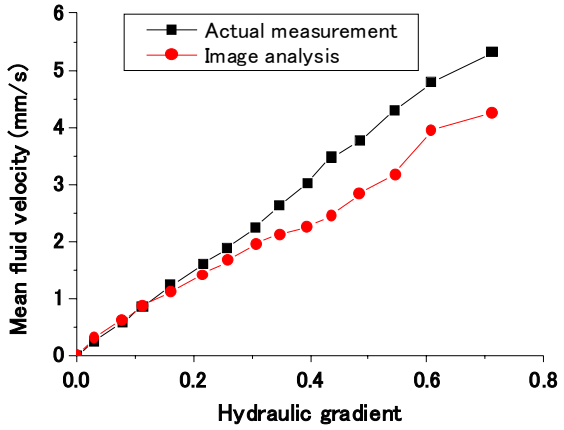

Fig.9 Comparison of vertical mean fluid velocity between actual measurement value and image analysis value.

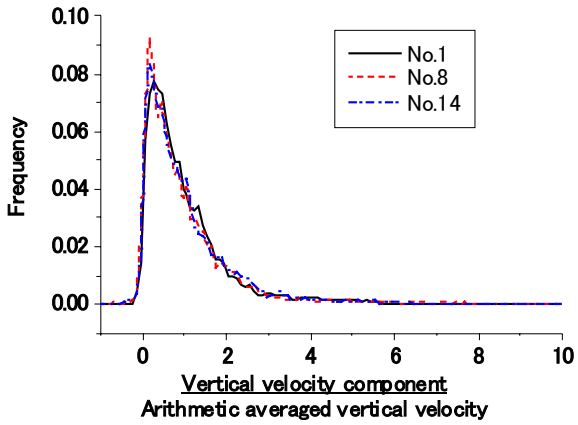

Fig.10 Histograms of vertical velocity component.

14. The values on the horizontal axis stand for dimensionless vertical velocities normalized by the arithmetic averaged vertical velocity. The three lines for different stages coincide well and obviously indicate a non-Gaussian distribution with a long tail reaching to almost 8 on the horizontal axis. The measured distribution curves seem to be simulated by a log-normal distribution.

The information about such non-Gaussian distribution is very useful in the Monte Carlo simulation often employed in modeling the long-term behavior of groundwater pollution.

(3) Pore fluid behavior during boiling

Once exceeding the critical stage represented by No. 14, a quick condition or boiling occurred in the specimen, and the hydraulic gradient stayed fairly constant despite the increase in the inflow rate. Meanwhile the layer consisting of the glass grains was entirely destroyed by the hydrodynamic force; both the glass grain and the silicone oil started to move randomly. Two hundreds photographs were taken at stage No.20 with 500 FPS (0.4 seconds in duration) and analyzed to clarify a complicate velocity field observed in boiling.

Figure 11 shows snapshots (left column) taken during the boiling together with the results of image analysis (right column). As shown in those figures, the LAT-PIV successfully captured a time series of localized upward flow in the region of 20 mm < x < 25 mm. This localized strong upward flow appeared with random width and it might be closely-linked to the local void ratio near the bottom of specimen.

Figure 12 represents the time history of the averaged vertical mean fluid velocity during the boiling. The figure indicates that even the averaged velocity fluctuated considerably during boiling. The time average value of the vertical mean fluid velocity was equal to 41.29 mm/s that is almost 3.4 times

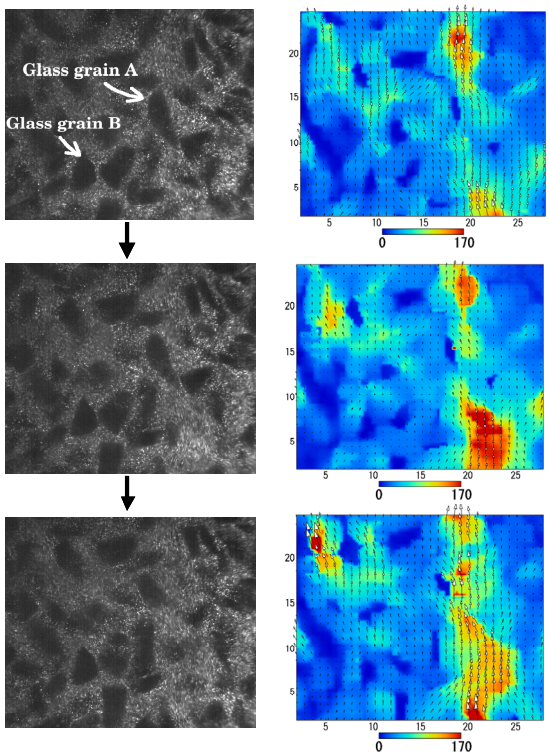

Fig.11 Snapshots of boiling.
(from top to bottom, t=0.198, 0.252, 0.306 s)

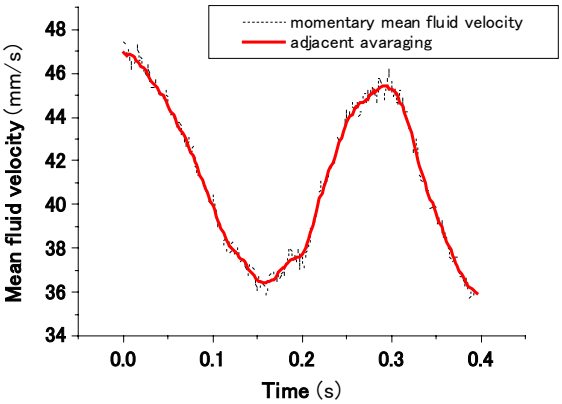

Fig.12 Vertical mean velocity during boiling.

grater than the experimental value obtained from the mass of outflow (12.26 mm/s).

Although the strong upward flow is captured in **Fig.11** from 0.2 s to 0.3 s, **Fig. 12** reveals that the averaged vertical velocity was rather smaller than that at the beginning of measurement, where no boiling was observed. The vertical fluid velocity was dominant in the range from 30 mm/s to 60 mm/s at the beginning of measurement, which resulted in the upward shift in the mean fluid velocity. At the time of 0.252 s, the strong upward flow invoked a little increase in the frequency of fluid velocity in the range from 140 mm/s to 165 mm/s; however, the frequency in the range from 15 mm/s to 40 mm/s was

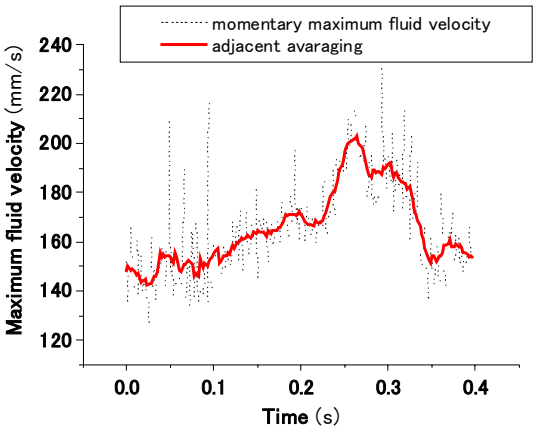

Fig.13 Vertical maximum velocity during boiling.

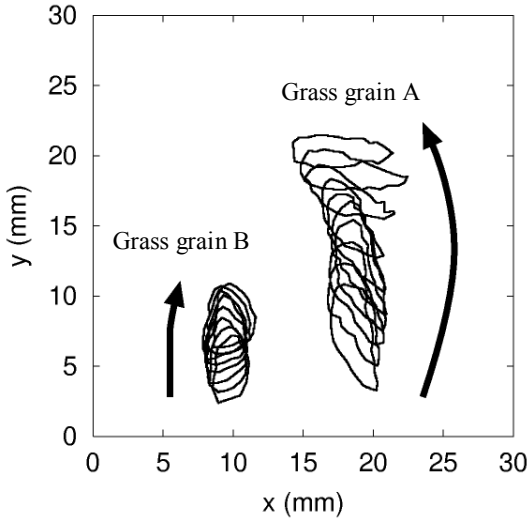

Fig.14 Trajectories of glass grains during boiling.

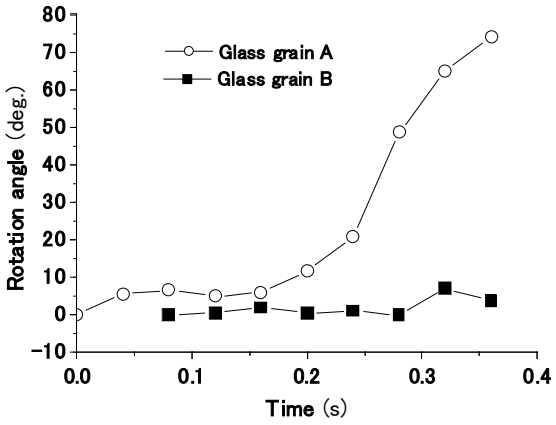

Fig.15 Rotation angles of glass grain A and B.

still high so that the mean fluid velocity was smaller than the value marked at the beginning of measurement.

Figure 13 traces the change in the maximum vertical velocity obtained from the image sets. The maximum vertical velocity was high in the time range from 0.2 s to 0.3 s, corresponding to the occurrence of boiling. The Reynolds number, calculated from the mean grain diameter, the fluid viscosity and the maximum vertical velocity component (203.07 mm/s at 0.264 s), was as low as 35; this small value suggests that the intense upward flow during boiling still remained in a laminar flow state.

(4) Measurement of glass grain behavior during boiling

The LAT-PIV also enables us to quantify the behavior of glass grains by tracing the boundaries between the fluorescent powder regions and the no pattern regions with the help of a GUI incorporating a semiautomatic edge detection program[10].

Figure 14 illustrates the trajectories of two glass grains A and B which are indicated in **Fig. 11**. **Figure 15** shows the change in their rotation angle with time. There was an obvious difference in the behaviors of these two grains. The grain A was acutely under the influence of the strong upward flow, causing a heavy anticlockwise rotation reaching to almost 70 degrees and a considerable translation within 0.4 seconds. On the other hand, the glass grain B, being positioned out of the strong upward flow, exhibited much less rotation and translation compared with grain A in spite of the small distance between them.

As abovementioned the LAT-PIV technique provides us with attractive information on the behavior of the particle-fluid system. It also has an advantage in terms of scalability, because the resolution shall easily be improved with rapid innovation of digital technology such as those employed in CCD cameras.

5. CONCLUSIONS

A visualization technique for the particle-fluid system, the LAT-PIV, was developed and applied to permeability tests including seepage failure. The test results are as follows:

1) The measured data proved that the Ergun's equation is able to represent the relationship between the mean fluid velocity and the hydraulic gradient with a good accuracy during the seepage state. However it was not applicable to the state of flow whose hydraulic gradient exceeds the critical value.
2) The frequency distribution of the fluid velocity during seepage state was quantified by the LAT-PIV, and consequently it is clearly recognized as a non-Gaussian distribution having a long tail which reaches 8 times of the mean fluid velocity.

3) The distribution of the fluid velocity during boiling was also quantified, and then the Reynolds number was calculated on the basis of the maximum vertical component. The Reynolds number was found to be almost 35, which indicated a laminar flow state.
4) The behaviors of glass grains during the boiling was quantitatively captured by means of a GUI equipped with a semiautomatic edge detection program.

Since the LAT-PIV is essentially a two-dimensional visualization technique, its development for the three-dimensional problems remains as a future prospect. In order to build up a three-dimensional visualization technique based on the LAT-PIV, such technique as stereo-PIV may be applicable.

ACKNOWLEDGMENT: The authors would like to thank Dr. Miyata (National Defense Academy in Japan) and Dr. Suetsugu (Saga University) for their encouragement and valuable suggestions on this study.

REFERENCES

1) Otani, J. : State of the art report on geotechnical X-ray CT research at Kumamoto University, *X-ray for Geomaterials; Soils, Concrete, Rocks –Otani & Obara (eds.)*, Swets & Zeitlinger, pp.43-77, 2004.
2) Kiyama, S. and Aoyama, S. : Microscopic Investigation from Crack Propagation to Shear Band of a Gravel Soil at Uniaxial Compression by CT Image, *X-ray for Geomaterials; Soils, Concrete, Rocks –Otani & Obara (eds.)*, Swets & Zeitlinger, pp.127-132, 2004.
3) Kobayashi, S., Takahashi, G. and Sekiguchi, H.: Visualization of the Dynamic Interactions of Granular Media-Pore Fluid Systems by X-ray TV Imaging, *Journal of Applied Mechanics*, JSCE, Vol. 3, pp. 521-531, 2000. (in Japanese)
4) Ogawa, K., Matsuka, T., Hirai, S. and Okazaki, K.: Three-dimensional Velocity Measurement of Complex Interstitial Flows Through Water-saturated Porous Media by the Tagging Method in the MRI Technique, *Meas. Sci. Technol*., 12, pp. 172-180, 2001.
5) Matsui, G., Mishiro, K., Monji, H., Tanaka, M. and Kamide, H. : Flow Characteristics in Channel with Local Blockage Packed with Spheres, *5th World Conference on Experimental Heat Transfer, Fluid Mechanics, and Thermodynamics*, pp. 24-28, 2001.
6) Sakakibara, J., Nakagawa, M. and Yoshida, M.: Stereo-PIV Study of Flow around a Maneuvering Fish, *Experiments in Fluids*, Vol. 36, pp. 282-293, 2004.
7) Konagai, K., Tamura, C., Rangelow, P. and Matsushima, T.: Laser-Aided Tomography: A Tool for Visualization of Changes in the Fabric of Granular Assemblage, *Structural Engineering / Earthquake Engineering*, Vol. 9, No. 3, pp. 192-201, JSCE, 1992.
8) Matsushima, T., Ishii, T. and Konagai, K.: Visualization of Three Dimensional Fabric in Granular Material by LAT, *The 6th Computer Visualization Symposium*, pp. 37-40, 2000. (in Japanese)
9) Matsushima, T., Saomoto, H., Tsubokawa, Y. and Yamada, Y.: Grain Rotation versus Continuum Rotation during Shear Deformation of Granular Assembly, *Soils & Foundations*, Vol. 43, No. 4, pp. 95-106, 2003.
10) Saomoto, H.: Experimental Observation and Direct Simulation of Particle-Fluid System, Doctoral Dissertation of University of Tsukuba, 2004.(in Japanese)
11) Ergun, S.: Fluid Flow Through Packed Columns, *Chemical Engineering Progress*, Vol. 48, No. 2, pp. 89-94, 1952.
12) McCabe, W., Smith, J., and Harriot, P.: *Unit Operations of Chemical Engineering*, McGraw-Hill, 2000.
13) Perry, R. H., Green, D. W. and Maloney, J.O.: *Perry's Chemical Engineers' Handbook*, McGraw-Hill, 1997.
14) Cheng, N. S.: Application of Ergun Equation to Computation of Critical Shear Velocity Subjected to Seepage, *Journal of Irrigation and Drainage Engineering*, ASCE, Vol.129, No.4, pp. 278-283, 2003.
15) Raffel, M., Willert, C. and Kompenhans, J.: *Particle Image Velocimetry, a Practical Guide*, Springer, 2000.

(Received February 6, 2007)